

# Low-temperature Thermal Expansion Anomalies in Indium and Its Solid Solution Alloys with Thallium\*

M. Liu,<sup>A</sup> T. R. Finlayson<sup>A</sup> and T. F. Smith<sup>B</sup>

<sup>A</sup> Department of Physics, Monash University, Clayton, Vic. 3168, Australia.

<sup>B</sup> Vice-Chancellor's Department, La Trobe University, Melbourne, Vic. 3083, Australia.

## Abstract

Low-temperature thermal expansion measurements have been made for fct, solid solution indium–thallium single-crystal alloys containing 6, 19, 24 and 29 at.% Tl. The expansion coefficients along the  $a$  and  $c$  axes for the 6, 19 and 24% alloys follow the same anomalous variations with temperature below about 15 K as for those of pure indium, with no change in magnitude. This contrasts with an increased magnitude for the anomalies previously reported for an In26.5at.%Tl alloy and reported here for the  $a$ -axis expansion for In29at.%Tl. These observations are discussed in terms of the Fermi surface topology for indium and their implications for the fcc to fct transformation in In–Tl alloys being electronically driven.

## 1. Introduction

Although indium crystallises with a face-centred tetragonal structure (fct) that is only moderately distorted from face-centred cubic (fcc), it exhibits considerable anisotropy in its thermal expansion (Collins *et al.* 1967). The low-temperature thermal expansion is particularly anomalous in that the crystal lattice initially contracts along the tetragonal  $c$  axis on heating below 5 K, whereas it expands along the  $a$  axis. While  $\alpha_a$  and  $\alpha_c$ , the  $a$ -axis and  $c$ -axis linear expansion coefficients, have quite complex temperature dependences, the volume coefficient  $\beta = 2\alpha_a + \alpha_c$  follows a normal temperature dependence.

Collins *et al.* noted that the near balance of elastic terms of opposite sign results in a sensitivity of  $\alpha_a$  and  $\alpha_c$  to small variations of the strain dependences of the crystal energy with temperature. This behaviour has also been discussed by Munn (1969), who arrived at a similar conclusion. Nevertheless, as pointed out by Collins *et al.*, this 'still leaves the microscopic origin a mystery'.

Indium and thallium form a continuous series of fct solid solution alloys, up to approximately 31 at.% Tl (Meyerhoff and Smith 1963; Luo *et al.* 1965; Pollock and King 1968). Between 0 and approximately 15 at.% Tl the fct phase crystallises directly from the melt. At higher Tl concentrations, the alloys solidify with the fcc structure and then undergo a martensitic transformation to the fct structure on cooling. The martensitic transformation temperature,  $T_M$ , varies sharply with composition, extrapolating to 0 K at the compositional limit of the fct phase.

\* Paper presented at the Festschrift Symposium for Dr Geoffrey Fletcher, Monash University, 11 December 1992.

In the course of studying the martensitic transformation in an In26·5at.%Tl alloy by thermal expansion measurements, it was observed that the low-temperature linear expansion coefficients followed very similar temperature dependences to those for indium, but were approximately four times larger in magnitude (Liu *et al.* 1990, 1993). In this paper these low-temperature measurements are described in more detail, along with new data that have been collected for In-Tl alloys containing 6, 19, 24 and 29 at.% Tl.

## 2. Experimental Details

### (2a) Sample Preparation

The 6 at.% Tl sample was spark-cut from a large cylindrical single crystal of about 25 mm diameter and 100 mm length. The crystal and the information on its composition were supplied by Dr H. G. Smith (1991, personal communication), Oak Ridge National Laboratory. The nominal composition of the crystal was 10 at.% Tl, but an electron-probe analysis gave a value of  $(5.6 \pm 0.4)$  at.% Tl, consistent with that ( $\sim 6$  at.% Tl) determined by measuring the flotation density of the crystal and referring it to the compositional dependence of density reported by Brassington and Saunders (1983) for In-Tl.

The 19, 26·5 and 29 at.% Tl alloy crystals were grown using a modified Bridgman method. The as-grown crystals were cylinders of approximately 10 mm diameter and 40–70 mm long. The actual composition for each crystal, determined by density measurement, was close to the nominal composition.

The samples spark-cut from the above crystals were approximate cubes with the edges parallel to tetragonal axes or cubic  $\langle 100 \rangle$  axes where applicable. Alignment prior to final spark-planing of each of the faces was accomplished within 1–2 degrees of the desired direction by the conventional X-ray Laue method. The dimensions of the cut crystals were from 4 to 7 mm.

The 24 at.% Tl single crystal was a parallel-sided piece cut from a much larger single crystal previously used for inelastic neutron scattering measurements (Finlayson *et al.* 1985), during which it had been repeatedly thermally cycled through the transformation below room temperature. The crystal preparation has been described in this previous publication. The piece used in the present thermal expansion studies was 3 mm thick with sides about  $12 \times 16$  mm<sup>2</sup> in area, which were approximately parallel to  $\{100\}_c$  ( $c = \text{cubic}$ ) planes.

### (2b) Applied Stress Field

For the samples with 19 at.% and higher Tl contents, the tetragonal structure is formed by a martensitic transformation from the fcc phase on cooling. Under normal conditions the complex microstructure of martensite twin bands which occurs in the transformed crystal would prevent pure, tetragonal  $a$ - or  $c$ -axis thermal expansion being measured. This was overcome for the 19, 26·5 and 29 at.% Tl samples by applying an appropriate external stress field to the sample to reduce the number of martensite variants or even to induce a single tetragonal domain (Liu *et al.* 1993).

It has been reported for the 26·5 at.% Tl that when a moderate uniaxial compressive stress, arising from the sample-loading springs of the capacitance dilatometer, was applied to the sample along the measurement direction  $l$ , the

sample was forced to transform on cooling such that this direction became a tetragonal  $a$  axis (Liu *et al.* 1993). Although there could still be one or two sets of martensite twin bands in the crystals, tetragonal  $a$ -axis behaviour was measured.

A biaxial-stress clamp was used for measurements of the tetragonal  $c$  axis. The cube-shaped sample was clamped with stresses applied along two cubic  $\langle 100 \rangle$  directions perpendicular to the third  $\langle 100 \rangle$ , which was also the  $l$  direction. The biaxial stresses were much greater than the stress from the loading springs, which, unavoidably, was present in all the cases along  $l$ . Thus, on cooling, a single, tetragonal domain was formed in the crystal below the transformation temperature and the tetragonal  $c$  axis was measured.

### (2c) Thermal Expansion Measurements

The low-temperature thermal expansion measurements were made in a three-terminal capacitance dilatometer identical to the design of White and Collins (1972). The data were collected on heating for temperatures  $>4.2$  K and on cooling for  $4.2-2$  K. The details of the measurements for each sample are given in the next section accompanying the corresponding results.

## 3. Results

As all measurements were made in zero magnetic field, below approximately 3.4 K the samples were in the superconducting state. The discontinuities in the linear expansion coefficients for indium at the superconducting transition, reported by Collins *et al.* (1967), are approximately one tenth of the size of  $\alpha_a$  and  $\alpha_c$ . A discontinuity of this size would not have been resolved in the present measurements.

The low-temperature thermal expansion coefficients for the In-Tl solid solution alloys are shown in Figs 1-6. The expansion behaviour for indium in the normal state (Collins *et al.* 1967) is shown in each figure for comparison.

### *In6at.%Tl*

The expansion measurements for the In6at.%Tl presented no difficulties as the tetragonal phase forms directly from the melt. The low-temperature expansion behaviour, which is shown in Fig. 1, is essentially identical to that of indium.

### *In19at.%Tl*

In its initial condition the 19 at.% Tl alloy crystal was twinned at room temperature after cooling through the transformation at  $\sim 80^\circ\text{C}$ . It was observed under an optical microscope that one set of twin bands existed in the crystal. According to Bowles *et al.* (1950) these should be parallel to one set of high-temperature cubic-phase  $\{110\}$  planes. Initial thermal expansion measurements made in a direction perpendicular to the surface on which the twin bands were observed followed  $c$ -axis behaviour. These are shown in Fig. 2. Following these measurements, the sample was clamped uniaxially, heated under vacuum in an oil-bath to  $\sim 120^\circ\text{C}$  and cooled back to room temperature to induce the formation of an  $a$  axis along the same  $l$  direction. Following this heat treatment, the crystal dimension in this direction had reduced by about 1.6%, indicating the formation

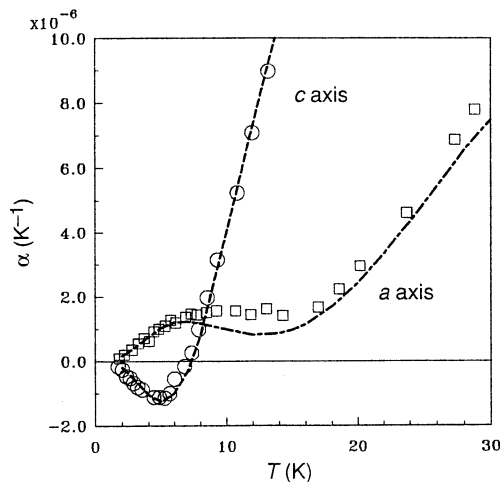


Fig. 1. Linear thermal expansion coefficients along the *a* axis ( $\square$ ) and *c* axis ( $\circ$ ) for In6at.%Tl as functions of temperature. The broken curves represent the variation of the corresponding linear expansion coefficients for In (Collins *et al.* 1967) in the normal state.

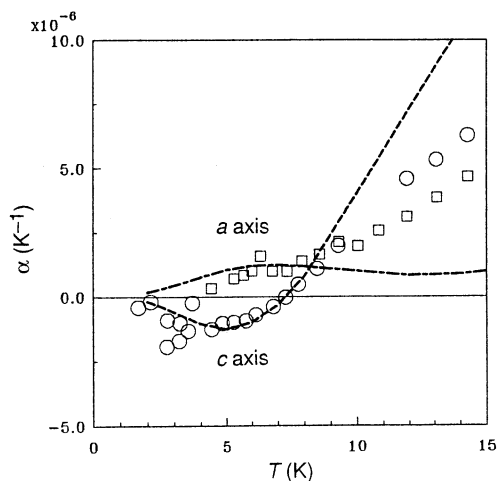


Fig. 2. As for Fig. 1 but for In19at.%Tl.

of the *a* axis. The *a*-axis data are also shown in Fig. 2. Although the data are more scattered than those for the In6at.%Tl crystal, it is clear that there again is no substantial difference between the expansion behaviour of the alloy and that for indium below about 9 K.

#### *In24at.%Tl*

The 24 at.% Tl sample and the others with higher Tl contents were in the fcc phase at room temperature. As noted above, this sample was irregular in shape

and consequently could not be clamped. Measurements were only made along a  $\langle 100 \rangle_c$  direction under the uniaxial stress from the loading springs. Although the uniaxial stress was present in this case, it was  $c$ -axis behaviour that was measured at low temperatures. The expansion behaviour in the vicinity of the transformation (190 K) was more consistent with the formation of the  $a$  axis in the  $l$  direction. It is assumed that on further cooling, the uniaxial stress was insufficient to control the crystal morphology on account of the relatively large surface area. This does leave some uncertainty as to the crystal direction for the measurements.

The expansion data are shown in Fig. 3 and again the  $c$ -axis expansion coefficient has a temperature dependence that is close to that for indium.

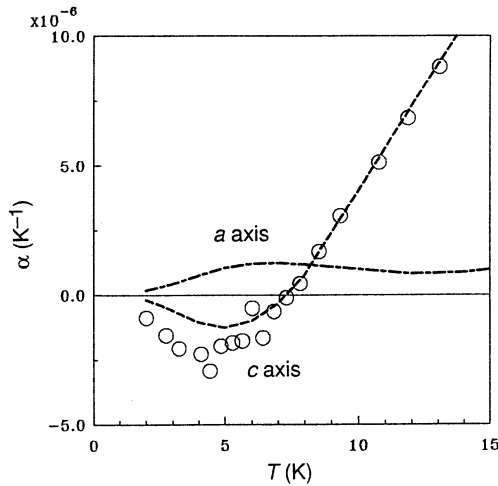


Fig. 3. As for Fig. 1 but for In24at.%Tl ( $c$ -axis only).

#### In26.5at.%Tl

The tetragonal  $a$ - and  $c$ -axis measurements for In26.5at.%Tl composition were made on two samples cut from the same single-crystal ingot. These data have been published previously in conjunction with a study of the fcc-fct transformation that occurs at around 105 K (Liu *et al.* 1993). The selection of the crystallographic axis as the measurement direction in the fct phase was determined by the external stress applied to each sample. The  $a$ -axis measurements were made on one crystal with the uniaxial stress in the measurement direction due to its spring-loaded mounting in the expansion cell. The  $c$ -axis measurements were made on the second crystal with an additional larger biaxial stress applied perpendicularly to the measuring direction.

The low-temperature thermal expansion data for In26.5at.%Tl are shown in Fig. 4. It is quite clear that although the temperature dependences for the expansion coefficients for the  $a$  and  $c$  axes are very similar to the temperature dependences for the corresponding directions in indium, the coefficients are approximately four times larger in magnitude.

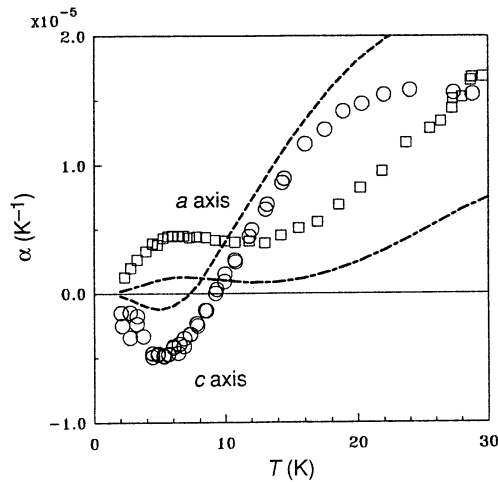


Fig. 4. As for Fig. 1 but for In26.5at.%Tl.

Collins *et al.* noted that although the linear expansion coefficients for indium were highly anisotropic, the volume coefficient  $\beta = 2\alpha_a + \alpha_c$  shows no unusual features. Indium is superconducting below 3.4 K. The volume coefficient in the normal state may be represented as

$$10^8 \beta = (0.66 \pm 0.2)T + (0.52 \pm 0.02)T^3 \text{ K}^{-1} \quad (1)$$

for  $T < 3.5$  K. The volume expansion coefficient derived from smooth fits to the data for  $\alpha_a$  and  $\alpha_c$ , plotted as  $\beta/3T$  as a function of  $T^2$  for In26.5at.%Tl, is presented in Fig. 5. The line represented by (1) for  $T < 3.5$  K is also shown. Although the uncertainty in the data points is large and the alloy data below 3.2 K are taken in the superconducting state\*, it is evident that the volume expansion coefficients of the alloy for  $T < 3.5$  K are essentially the same as those for indium. Thus, while the low-temperature linear expansion coefficients for the In26.5at.%Tl are approximately four times larger than those for indium, the corresponding increase in the tetragonality of the alloy on cooling, relative to that for In, occurs without any relative change in the volume.

#### In29at.%Tl

The initial thermal expansion measurements on the In29at.%Tl sample subjected to the uniaxial stress due to the spring-loaded sample mounting showed *a*-axis behaviour identical to that reported for the In26.5at.%Tl sample, but with a  $T_M \sim 60$  K. The low-temperature expansion behaviour is shown in Fig. 6, where it is compared with those for In26.5at.%Tl, In6at.%Tl and indium. While the form of the behaviour for all four compositions is similar there is a considerable further increase in the magnitude of  $\alpha_a$  above that for In26.5at.%Tl and amounting to approximately an order of magnitude larger values than for In below  $\sim 15$  K.

\* The fall-off of  $\beta$  below approximately 2.6 K may be due to a decline of the electronic component below  $T_c$ .

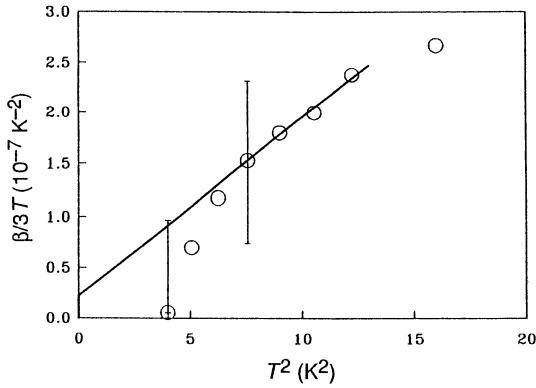


**Fig. 5.** Volume expansion coefficient  $\beta$  for In26.5at.%Tl plotted in the form  $\beta/3T$  against  $T^2$ . The line represents the variation of the volume coefficient for indium in the normal state derived from expression (1).

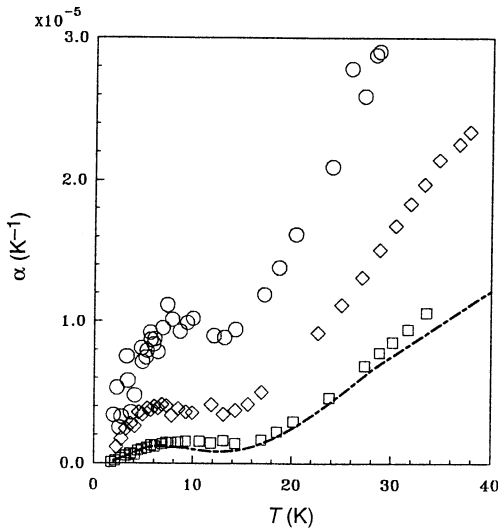


**Fig. 6.** The  $a$ -axis thermal expansion coefficients as functions of temperature for In29at.%Tl ( $\circ$ ), In26.5at.%Tl ( $\diamond$ ) and In6at.%Tl ( $\square$ ). The broken curve represents the variation of  $\alpha_a$  for In (Collins *et al.* 1967).

It was noted that it took significantly longer to reach a stable capacitance reading from the expansion cell between successive readings than for the other alloys. This is attributed to the transformation being incomplete down to 2 K, which would be consistent with the phase diagram for this composition (Pollock and King 1968).

An attempt to induce a single-domain fct crystal for measurements along the  $c$  axis, by application of a biaxial stress, as was done for In26.5at.%Tl, was unsuccessful as judged from the magnitude of the transformation strain.

Furthermore, the strain changed erratically with change of temperature below  $\sim 10$  K, and below 4.2 K the sample expanded so much that the gap in the expansion cell closed. This suggests that the transformation temperature may have been displaced to a lower temperature under the influence of the biaxial stress.

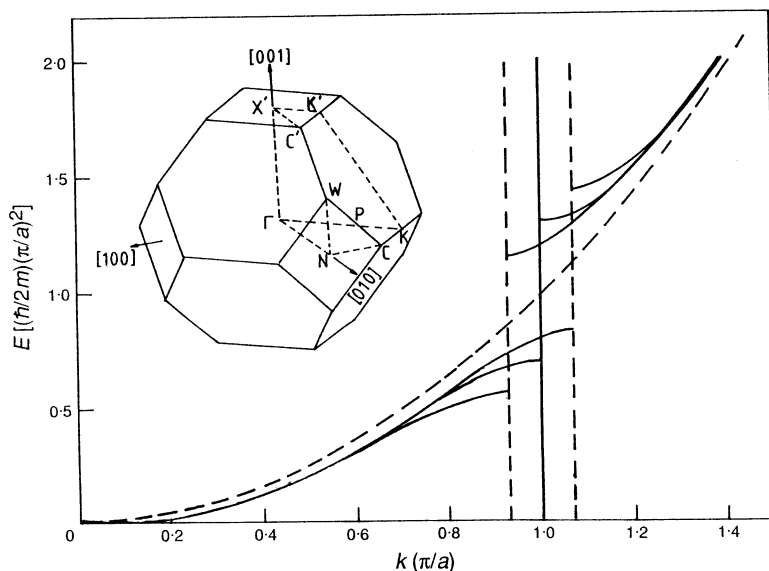


Fig. 7. Schematic representation of the Brillouin zone boundary-Fermi surface interaction at the  $C'$ ,  $W$  and  $C$  points by comparison with a free-electron energy band (dashed curve). The Brillouin zone for the fcc lattice is shown in the insert.

#### 4. Discussion

The distortion from the fcc structure that occurs in indium and a number of its solid solution alloys has been explained by Yonemitsu (1966) in terms of a simple free-electron model. This followed an earlier suggestion by Tyzack and Raynor (1954) that overlap of the Fermi sphere with the Brillouin zone boundary was responsible for the distortion.

The Brillouin zone for the fcc lattice is shown in Fig. 7. In the free-electron approximation the Fermi surface for a trivalent atom just touches the second-zone boundary at  $W$ , producing a large second-zone surface and overlaps into the third zone along the  $\langle 110 \rangle$  edges, to form electron 'arms'. Additional electron pockets also occur in the fourth zone (Harrison 1960).

The distortion to the fct lattice means that the symmetry points  $C'$ ,  $W$  and  $C$ , and  $K$  and  $K'$ , are no longer equivalent. This results in a free-electron Fermi surface for indium, where the third-zone electron arms are no longer connected at  $C$ . While this free-electron surface is quite close to the measured surface, there are several differences (Holtham 1976). The Fermi surface derived from a number of experimental techniques consists of a closed second-zone hole surface and third-zone electron 'arms' ( $\beta$ -arms) along the  $[110]$  edges. The details of the

connectivity of the Fermi surface are critically dependent upon the position of the energy bands at the points  $C$ ,  $C'$  and  $W$ , which are sensitive to the relative magnitudes of the  $V_{111}$ ,  $V_{200}$  and  $V_{002}$  Fourier components of the pseudopotential.

Crystal-lattice distortion due to Fermi surface-Brillouin zone overlap was first discussed by Jones (1934) and later by Goodenough (1953). The effect, which is shown schematically in Fig. 7, may be thought of as a balance between the crystal-lattice energy (elastic energy) and the electronic kinetic energy (band energy).

As the Fermi surface approaches the Brillouin zone boundary the energy of the nearly full band may be lowered by distorting the Brillouin zone to bring the boundary closer to the Fermi surface. This may be expressed as an effective attraction between the Fermi surface and the zone boundary. Once the Fermi surface touches the zone boundary it becomes energetically more favourable to prevent higher energy states being filled by overlap, which results in an effective repulsion between the electron surface and the zone boundary. Thus for indium the tetragonal distortion is expected to be a result of a balance in the forces acting between the Brillouin -zone boundary and the second-zone hole and third-zone electron surfaces.

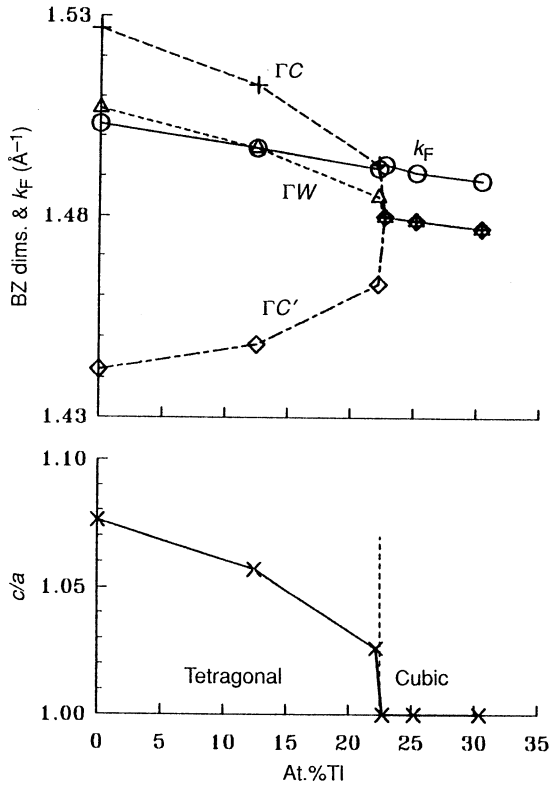
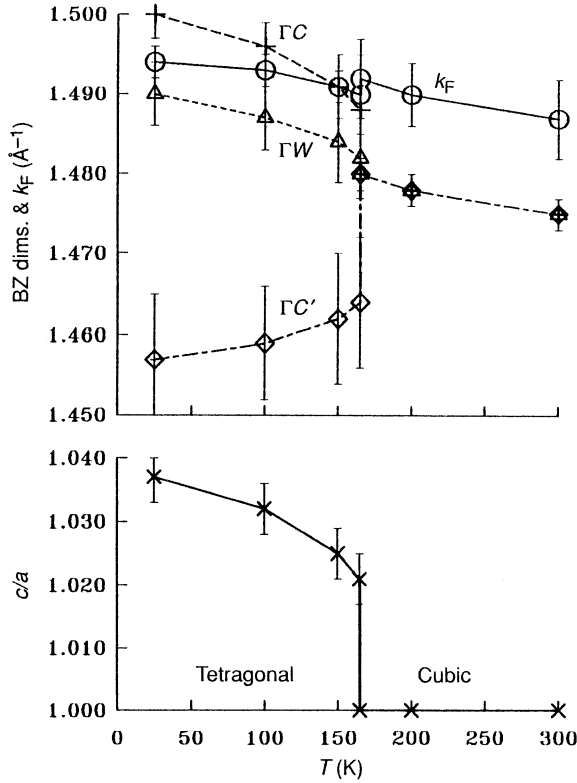


Fig. 8. Brillouin zone dimensions, free-electron Fermi surface radius and  $c/a$  as functions of Tl concentration for In-Tl alloys at room temperature, derived from the X-ray data of Guttman (1950).



**Fig. 9.** Brillouin zone dimensions, free-electron Fermi surface radius and  $c/a$  for In26.5at.%Tl as functions of temperature, derived from the X-ray data of Donovan (1991).

Alloying thallium with indium is not expected, to a first approximation, to alter the electronic structure as both elements are trivalent. Nevertheless, the  $c/a$  ratio decreases, causing the zone boundary to move closer to the Fermi surface at  $C$ ,  $C'$  and  $W$  (see Fig. 8). This results in a narrowing of the  $\beta$  arms at  $C'$ , but overlap at  $C$  does not occur until the fct to fcc transformation, which occurs at 22.7 at.% Tl at room temperature. Overlap does occur at  $W$  for alloys with Tl  $\geq 12.5$  at.%. Similar behaviour is seen as the fct to fcc transformation is approached as a function of temperature for In26.5at.%Tl (Fig. 9). Again the transformation occurs just as the Fermi surface touches at  $C$ . We conclude that the alloying of thallium with indium reduces the energy advantage derived by reducing the third-zone overlap through the lattice distortion, presumably because of changes in the pseudopotential. Furthermore, for compositions greater than 15 at.% Tl the energy due to thermal disorder is large enough to offset the electronic energy gain before melting, and this leads to the temperature-dependent martensitic fct-fcc transformation.

The low-temperature thermal expansion for In and In-Tl reinforces the picture of an electronically driven distortion. As  $T \rightarrow 0$  and the electronic thermal excitation energy dominates, the tetragonal distortion *increases*. Furthermore,

as the Fermi surface gets closer to the zone boundary, the effect is significantly increased, whereas the volume expansion is unchanged. This picture of an electronically driven distortion is consistent with the peak in the electronic density of states, which has been reported (Munukutla and Cappelletti 1980) for In<sub>31</sub>at.%Tl, the approximate compositional limit for the fct phase. It is also consistent with the peak that occurs in the superconducting transition temperature (Luo *et al.* 1965) at the same composition.

Smith (1973) has discussed the evidence for changes in the connectivity of the indium Fermi surface due to changing the electron per atom ratio by alloying. In particular it was argued that addition of approximately 1.5 at.% Cd results in the pinching off of the  $\beta$  arms at  $C'$ . The fct-fcc boundary occurs at 6 at.% Cd at room temperature (Heumann and Predel 1962; Merriam 1966). We propose to measure the low-temperature thermal expansion of In-Cd alloys to investigate further the influence of the Fermi surface connectivity on the crystal stability.

## 5. Conclusion

It has been concluded from measurements on indium alloyed with thallium that the anomalous low-temperature thermal expansion for indium is due to the overlap of the Fermi surface between the second and third Brillouin zones. Minimisation of the electronic energy associated with the zone overlap is responsible for the tetragonal distortion of indium and indium-thallium alloys up to 31 at.% Tl. It is proposed that the offsetting of the electronic energy by the thermal disorder energy for alloys containing more than 15 at.% Tl results in the temperature-dependent martensitic fct-fcc transformation.

## Acknowledgments

The 6 at.% Tl alloy crystal was kindly provided by Dr H. G. Smith of Oak Ridge National Laboratory, and the electron-probe analysis for this crystal was performed by Mr R. J. Liebach. The partial support provided by the Australian Research Council is gratefully acknowledged.

## References

- Bowles, J. S., Barrett, C. S., and Guttman, L. (1950). *J. Metals* **188**, 1478.
- Brassington, M. P., and Saunders, G. A. (1983). *Proc. R. Soc. London A* **387**, 289.
- Collins, J. G., Cowan, J. A., and White, G. K. (1967). *Cryogenics* **7**, 219.
- Donovan, D. W. (1991). Ph.D. thesis, Penn. State Univ., USA.
- Finlayson, T. R., Mostoller, M., Reichardt, W., and Smith, H. G. (1985). *Sol. State Commun.* **53**, 461.
- Goodenough, J. B. (1953). *Phys. Rev.* **89**, 282.
- Guttman, L. (1950). *J. Metals* **188**, 1472.
- Harrison, W. A. (1960). *Phys. Rev.* **118**, 1182.
- Heumann, T., and Predel, B. (1962). *Z. Metallk.* **53**, 240.
- Holtham, P. W. (1976). *J. Phys. F* **6**, 1457.
- Jones, H. (1934). *Proc. R. Soc. London A* **147**, 396.
- Liu, M., Finlayson, T. R., and Smith, T. F. (1990). *Mater. Sci. Forum* **56-8**, 311.
- Liu, M., Finlayson, T. R., and Smith, T. F. (1993). *Phys. Rev. B* (in press).
- Luo, H. L., Hagen, J., and Merriam, M. F. (1965). *Acta Metall.* **13**, 1012.
- Merriam, M. F. (1966). *Phys. Rev.* **144**, 300.
- Meyerhoff, R. W., and Smith, J. F. (1963). *Acta Metall.* **11**, 529.

- Munn, R. W. (1969). *Adv. Phys.* **18**, 515.  
Munukutla, L. V., and Cappelletti, R. L. (1980). *Phys. Rev. B* **21**, 5111.  
Pollock, J. T. A., and King, H. W. (1968). *J. Mater. Sci.* **3**, 372.  
Smith, T. F. (1973). *J. Low Temp. Phys.* **11**, 581.  
Tyzack, C., and Raynor, G. V. (1954). *Trans. Faraday Soc.* **50**, 675.  
White, G. K., and Collins, J. G. (1972). *J. Low Temp. Phys.* **7**, 43.  
Yonemitsu, K. (1966). *J. Phys. Soc. Jpn* **21**, 1231.

Manuscript received 26 February, accepted 23 June 1993